analytical chemistry

Article

Cite This: Anal. Chem. 2018, 90, 6229−6239

pubs.acs.org/ac

Analysis of Crystalline Silica Aerosol Using Portable Raman Spectrometry: Feasibility of Near Real-Time Measurement

Lina Zheng, Pramod Kulkarni,* M. Eileen Birch, Kevin Ashley, and Shijun Wei

Centers for Disease Control and Prevention, National Institute for Occupational Safety and Health, Cincinnati, Ohio 45226, United States

Supporting Information

ABSTRACT: A Raman spectroscopy based method has been developed for measurement of trace airborne concentrations of respirable crystalline silica (RCS) using various aerosol sampling and analysis techniques. Three aerosol microconcentration techniques were investigated for effective coupling of collected particulate samples with micro-Raman spectroscopy: (i) direct analysis on a particulate filter after focused aerosol collection using a converging nozzle; (ii) analysis of dried particulate deposit on a filter obtained directly from the aerosol phase using the Spotsampler device; and (iii) analysis of a dried spot (∼1−3 mm diameter) obtained by redepositing the particulate sample, after low-temperature plasma ashing of the filter sample. The deposition characteristics (i.e., spot diameter, shape, and deposit uniformity) of each technique were investigated. Calibration curves were constructed and detection limits were estimated for α-quartz using the A_1 Raman Si−O−Si stretching−bending phonon mode at 465 cm^{-1}. The measurement sensitivity could be substantially improved by increasing the signal integration time and by reducing the particle deposition area. Detection limits in the range of 8−55 ng could be achieved by microconcentrating the aerosol sample over a spot measuring 400−1000 μm in diameter. These detection limits were two to three orders of magnitude lower compared to those attainable using current standardized X-ray diffraction and infrared spectroscopy methods. The low detection limits suggest that near real-time measurements of RCS could be achieved with limits of quantification ranging from 2 to 18.5 $\mu g/m^3$ (at 10 min collection time and 1.2 L/min sampling flow rate), depending on microconcentration technique used. The method was successfully extended to the measurement of α-quartz air concentration in representative workplace aerosol samples. This study demonstrates the potential of portable micro-Raman spectroscopy for near-real time measurement of trace RCS in air.

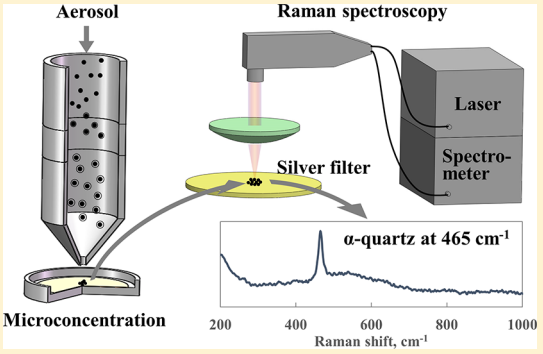

Occupational exposure to crystalline silica aerosol is common in construction, mining, and industrial activities such as cutting, grinding, or drilling silica containing materials, abrasive blasting, hydraulic fracturing, and foundries.[1−3] Approximately 2 million workers in the United States are exposed to respirable crystalline silica (RCS) in their workplaces each year.[4] Long-term inhalation of aerosol containing crystalline silica can cause silicosis and other serious lung diseases, including cancers.[2,3] For protection of workers' health, the U.S. Occupational Safety and Health Administration (OSHA) has recently issued a permissible exposure limit (PEL) for RCS of 50 $\mu g/m^3$ averaged over an 8 h workshift.[3] Accurate measurement of airborne crystalline silica concentrations is of great significance for preventing harmful exposures.

Current methods for measuring airborne RCS involve filter collection over several hours, followed by laboratory analysis using either X-ray diffraction (XRD)[5] or infrared (IR) spectroscopy.[6] Filter samples are usually pretreated using low temperature plasma ashing[7−9] or muffle furnace ashing[7−9] and subsequently redeposited on another filter to achieve a relatively uniform deposits for optimum presentation to the X-ray or infrared beam.[10,11] Direct on-filter techniques have also been used for RCS measurement, which do not require the sample pretreatment, but suffer from matrix interferences for some samples.[10,11] Limits of detection (LODs) for quartz obtained by current standardized XRD and IR methods range from 3 to 10 μg per sample.[7,8,12] In a workplace with RCS concentrations near the PEL, collection over several hours (h), typically 8 h, is usually required to obtain quantifiable mass loading per filter. Using current methods, it is difficult to capture short-term (even at relatively high levels) or task-specific exposures that are typical in workplaces. Developing more sensitive and field-portable methods for RCS measurement is desired for effective evaluation of human exposures and rapid implementation of exposure mitigation measures.

Raman spectroscopy is an attractive technique for chemical characterization of aerosols owing to its ability to selectively identify specific vibrational modes in organic and inorganic substances. Most studies describing aerosol analysis using Raman spectroscopy have focused on qualitative characterization of chemical components of individual particles,[13−17] or

Received: February 20, 2018
Accepted: April 16, 2018
Published: April 16, 2018

DOI: 10.1021/acs.analchem.8b00830
Anal. Chem. 2018, 90, 6229−6239

bulk particulate samples,[18−20] collected on a substrate. Quantitative analysis of aerosols using Raman spectroscopy is challenging due to the miniscule sample volume probed by the excitation laser. Although in situ measurements of chemical composition of suspended aerosol particles using this technique have been reported in several studies,[21−23] the detection limits are too high (greater than 1 mg/m^3) to be practically useful for trace-level measurements of atmospheric or workplace aerosols. Aerosol microconcentration, wherein airborne particles are deposited over a small (microscale) area of a collection substrate, has proven to be a useful technique for improving the measurement sensitivity for aerosol characterization using microscale spectroscopy, such as laser-induced breakdown spectroscopy,[24] spark emission spectroscopy,[25−29] glow discharge optical emission spectroscopy,[30] and quantum cascade laser-based infrared spectroscopy.[31] The objective of this study was to assess the effectiveness of various aerosol microconcentration techniques for trace measurement of airborne RCS using a "field-portable" Raman spectrometer.

Raman spectroscopy has been proven to be a useful analytical tool for trace measurement of RCS as well as distinguishing between polymorphs of crystalline silica.[32,33] Stacey et al. have recently reported limits of quantification (LOQs) between 0.066−0.161 μg for quartz when measuring samples deposited on a 5 mm diameter area on silver filters using a sensitive, research-grade, laboratory Raman microscope.[33] In this study, we employed a lightweight (<3.5 kg), field-portable Raman spectrometer and focused sample collection of RCS to achieve detection limits comparable to those reported by Stacey et al.[33] Because the excitation laser in micro-Raman spectroscopy interrogates a miniscule volume of sample over a small area (<1 to 100 μm in diameter), efficient microconcentration of aerosol samples to a narrow spot is critical for improving measurement sensitivity and reducing variability. For the first time, we report effective aerosol microconcentration techniques for sensitive Raman measurement of RCS. The deposition diameter, shape, and uniformity resulting from the proposed aerosol microconcentration methods were investigated. Calibration approaches were developed for Raman measurement of airborne α-quartz concentrations, and the methods were applied to measurement of actual workplace aerosol samples containing crystalline silica.

EXPERIMENTAL SECTION

Approaches for Raman Measurement of Aerosol. Figure 1 shows a schematic diagram of three approaches for aerosol measurement using Raman spectroscopy. Methods A and B are direct-on-filter analysis methods. Method A involves direct analysis of a spot sample on a particulate filter after focused aerosol collection using a converging nozzle. Method B involves analysis of a dried particulate spot sample on a filter obtained directly from the aerosol phase using the Spotsampler device[34] described later. Method C is a laboratory-based method requiring sample pretreatment prior to Raman measurement. It involves analysis of a particulate sample collected on a filter after ashing and resuspension as a colloid, followed by deposition as a small spot using syringe filtration. Additional details on these methods are provided in the next section.

Aerosol Microconcentration Techniques. Particulate filter samples used for Raman analysis were prepared using three aerosol microconcentration techniques illustrated in Figure 2. These techniques include the following: (i) focused collection over a small spot (≤1 mm diameter) using a converging nozzle[31] (Figure 2a; method A); (ii) focused collection over a very small spot (<0.5 mm diameter) using a condensational growth tube in a Spotsampler device (Figure 2b; method B); and (iii) filter sample redeposition, as a small spot (1−3 mm diameter), using several milliliters of a silica suspension prepared after low temperature plasma ashing of filter samples collected by conventional air sampling[9] (Figure 2c; method C).

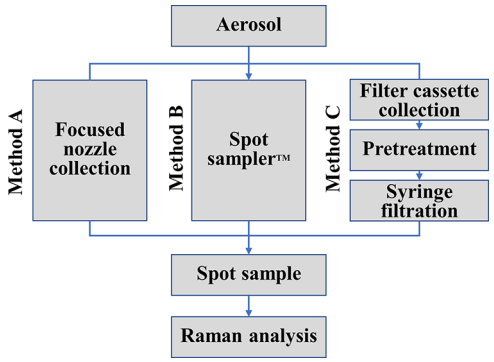

Figure 1. Schematic diagram of three approaches for aerosol measurement using Raman spectroscopy. Methods A and B are direct-on-filter methods requiring no sample pretreatment. These collection methods can be adopted into a continuous, automated real-time instrument. Method C is a laboratory method designed to minimize matrix interferences and involves sample pretreatment and redeposition prior to Raman analysis.

Three types of filters were investigated to ensure that there was no spectral interference in the Raman shift frequency range of interest: silver filter (0.8 μm pore size, SKC Inc.), polycarbonate (PC) filter (0.8 μm pore size, SKC Inc.), and polyvinyl chloride (PVC) filter (5 μm pore size, SKC Inc.).

For method A, a 25 mm diameter filter (silver, PC, or PVC filter) was housed in a 25 mm filter cassette (SKC Inc., Eighty Four, PA, U.S.A.), and a converging nozzle with a jet diameter of 0.8 mm was securely attached to the inlet of the filter cassette. A nonporous, rigid disc (made of polymer resin) with a center orifice (1 mm diameter) was placed beneath the filter supporting pad to reduce expansion of the aerosol flow exiting the nozzle. The particulate sample was collected onto the filter directly from the aerosol phase at a flow rate of 1.2 L min^{-1} using an air sampling pump (Model: GilAir Plus; Sensidyne, LP, St. Petersburg, FL, U.S.A.).

For method B, a Spotsampler device (Series 110, Aerosol Devices Inc., Fort Collins, CO, U.S.A.) was used for focused collection of particles directly from the aerosol phase. In this method, aerosol particles are grown into liquid droplets (>1 μm diameter) in a condensation growth tube;[34] and the grown droplets are subsequently collected on a solid substrate. The dried spots were collected on a 4 mm diameter filter punch, which were placed in sample collection wells. The particulate deposits were heat dried at 40 °C during sample collection in a heated well plate of the Spotsampler device. It is possible that, even after heat-drying, the particulate deposit may have contained trace levels of adsorbed or absorbed water, since complete drying and desorption may require much higher temperatures. However, no O−H stretching bands were observed in any of the Raman spectra, confirming that there was no interference from water. Dried spots of particulate matter were obtained at a flow rate of 1.2 L min^{-1}. It is noted

DOI: 10.1021/acs.analchem.8b00830
Anal. Chem. 2018, 90, 6229−6239

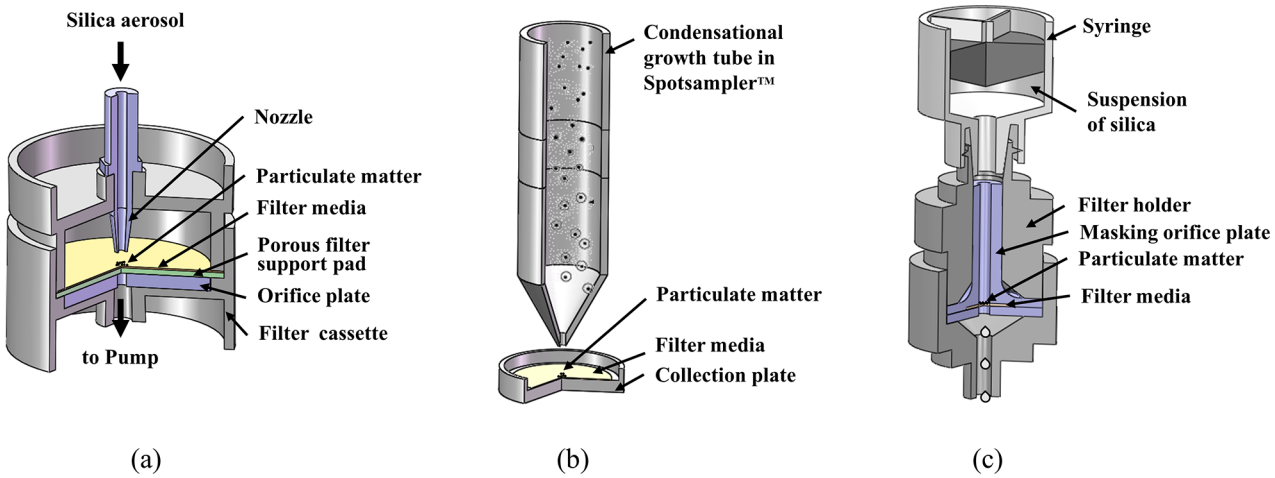

Figure 2. Three focused aerosol deposition techniques used in this study: (a) direct aerosol microconcentration using a converging nozzle; (b) direct aerosol microconcentration using a Spotsampler device; and (c) redeposition through a narrow orifice. See text for details.

the Spotsampler device used in method B is suitable for collecting area samples.

In method C, the analyte suspension was passed through the filter media using two masking orifice plates, placed on opposite sides of the filter (6 mm diameter), as shown in Figure 2c, such that the suspension was forced to filter only through the narrow orifice opening in the center, thereby masking the rest of the filter. The filter, which was sandwiched between the two masking orifice plates, was housed in a syringe-filter holder (13 mm diameter, stainless-steel; EMD Millipore, Darmstadt, Germany) with a Luer-lock fitting. Three pairs of masking orifice plates with different orifice diameters (i.e., 1, 1.5, and 3 mm) were designed to obtain different filter spot sizes. The analyte suspension was filled in a 10 mL syringe (Becton, Dickinson and Company, Franklin Lakes, NJ, U.S.A.) with a Luer-lock tip, which was then securely attached to the filter holder to allow the suspension to be filtered steadily without any leakage or filter rupture. Steady filtration of 10 mL took about 1 min.

Calibration Methods. For methods A and B, calibration aerosol was generated by aerosolizing MIN-U-SIL-5 fine ground silica powder (U.S. Silica Company, Frederick, MD, U.S.A.) at room conditions using a fluidized bed aerosol generator (Model 3400A; TSI Inc., Shoreview, MN, U.S.A.). The flow rate for aerosol collection in methods A and B was 1.2 L/min. The total particulate mass loading on a collection filter was determined from the measured aerosol mass concentration at the inlet of the collection device, the flow rate, and the collection time. The mass concentration of the test aerosol was measured using a piezobalance dust monitor (Series 3520; Kanomax USA, Inc., Andover, NJ, U.S.A.). For method C, suspensions of the standard reference material respirable quartz (SRM 1878a; NIST, Gaithersburg, MD, U.S.A.) with different concentrations of quartz ranging from 0.05 to 100 μg/mL, were prepared in ultrafiltered deionized water (CAS 7732−18−5, Thermo Fisher Scientific, Rochester, NY, U.S.A.). These suspensions were placed in an ultrasonic bath for 5 min before use. Prior to drawing the suspension into a 10 mL syringe, the suspension was agitated for 10−20 s using a vortex mixer (Barnstead Thermolyne Maxi-Mix Plus, Model# M63215). Then, 2 mL of each suspension were deposited onto a silver filter (6 mm diameter and 0.8 μm pore size) using the apparatus shown in Figure 2c. The filters were subsequently dried on a hot plate (100 °C) to obtain dried spot samples with known mass loadings. In all three methods, for a given mass loading, a minimum of three replicate samples were prepared.

The silica samples deposited on filters were analyzed using a portable Raman spectrometer (i-Raman; B&W Tek, Newark, DE, U.S.A.). The external dimensions of the instrument were 17 × 34 × 23.4 cm, and its weight was 3 kg. The spectrometer had a wavenumber range of 150−3200 cm^{-1} at a spectral resolution of 3.5 cm^{-1}. The excitation wavelength used in the instrument was 785 nm with a maximum power of 420 mW. The laser was focused onto the deposit using a 20× objective. The numerical aperture of the objective was 0.40. The working distance was 8.8 mm. The spot diameter of the area illuminated by the laser was approximately 105 μm. The Raman spectra were collected at a power of 420 mW of the excitation laser. Various integration times (4−30 s) were used depending on the mass loadings to obtain variation of Raman scattered intensity (I) as a function of wavelength of scattered light. The signal intensity for α-quartz was calculated as the peak height at a Raman shift of ≈465 cm^{-1} after baseline correction (I_p). For each filter sample, spectra were taken from three randomly selected locations and the mean signal intensity for each sample was obtained by averaging over these three measurements. Calibration curves were constructed by plotting the Raman signal intensity as a function of the silica mass loading on the filter.

Analysis of Workplace Samples. Two types of workplace aerosols containing α-quartz were tested by using collection methods A and C. These workplace dust samples (powders) were collected during cutting operations (using power tools) of building products (natural stone and fiber cement siding) at construction sites. The detailed experimental scheme for collecting test samples for Raman as well as reference method is shown in Figure S1 in the Supporting Information (SI). Test aerosols were generated in the laboratory by aerosolizing the workplace aerosol samples using a fluidized bed aerosol generator. The respirable fractions of test aerosol was obtained using a personal sampling cyclone (particle size cut PM_4 at 4.2 LPM; Model# GK2.69; Mesa Laboratories, Inc., Butler, NJ, U.S.A.). The total mass concentrations of the test aerosol were varied using a dilution device. Respirable test aerosols were microconcentrated by methods A and C described earlier (as shown in Figure 2) and analyzed by Raman spectroscopy. The

DOI: 10.1021/acs.analchem.8b00830
Anal. Chem. 2018, 90, 6229−6239

α-quartz mass loading for each collected aerosol sample was determined using the constructed calibration curves. The measured quartz mass was then converted to the air concentration ($\mu g/m^3$) of the test aerosol using the aerosol flow rate and the collection time.

In method A, respirable test aerosol was directly collected onto silver filters. The aerosol samples on the silver filters (25 mm diameter and 0.8 μm pore size) were then analyzed by a portable Raman spectrometer. In method C, respirable test aerosol was collected on MCE filters (0.8 μm pore size) housed in a 25 mm filter cassette. Following this collection, the filters were pretreated to minimize potential matrix interferences by using low temperature plasma ashing.[8,9] The MCE filter samples were placed in a 25 mL glass scintillation vial (PCM Surplus World) within a low-temperature plasma asher (Series 600, Anatech Ltd., Union City, CA, U.S.A.). The plasma asher was operated at 50 mL/min oxygen flow rate and 250 W power for 1.5 h. After complete ashing, 2 mL of DI water was carefully added to each vial, then the vial was sonicated for 5 min in an ultrasonic bath. The resulting suspension was transferred into a 10 mL syringe. The vial was rinsed with 1 mL DI water and the rinsate was also transferred into the syringe. The suspension was then deposited onto a silver filter using the apparatus shown in Figure 2c. The syringe filtration device was operated manually. The rate of filtration was approximately 0.2 mL/s.

RESULTS AND DISCUSSION

Laser-Induced Heating. Potential for thermal decomposition of sample due to laser-induced heating were investigated. Raman spectra for a given sample spot obtained at various laser power levels showed that the peak signal increased linearly with laser power (see Figure S2 in the SI). Additionally, at the highest laser power (420 mW), consecutive measurement of peak Raman signal for a given sample spot showed constant Raman signal with time (see Figure S3 in the SI). In these measurements, Raman signal was integrated for 4 s, followed by a wait period of 56 s during which the excitation laser remained on (and continued to irradiate the sample). The total Raman signal as a function time was approximately constant for up to 10 min (see Figure S3 in the SI). These measurements suggest that the laser-induced thermal heating was negligible for laser power up to 420 mW.

Effect of Filter Type on Analyte Signal. To investigate the effect of the filter media on the Raman signal, Raman spectra were measured using three types of filters at the same particulate mass loadings: silver, PC and PVC. Silver and PC filters were found to have no spectral interference with the α-quartz peak at 465 cm^{-1} and were subsequently used in the following experiments. Figure 3 shows Raman spectra of α-quartz deposited on silver and PC filters at different mass loadings using method A (i.e., focused, direct collection using a nozzle). For each filter type, the peak Raman signal intensity of α-quartz increased linearly with increasing filter loading. Comparison of the signal intensity from the silver and PC filters shows that the silver filter provided higher signal intensity for a given mass loading, which has been attributed to the enhanced Raman scattering from porous silver membrane filters used as substrates.[35]

Size and Uniformity of Particulate Deposit. As the excitation laser beam diameter is small compared to the sample spot diameter, only a miniscule portion of the sample deposit could be irradiated by the excitation laser. To ensure that the mass is accurately measured with high precision, it is essential

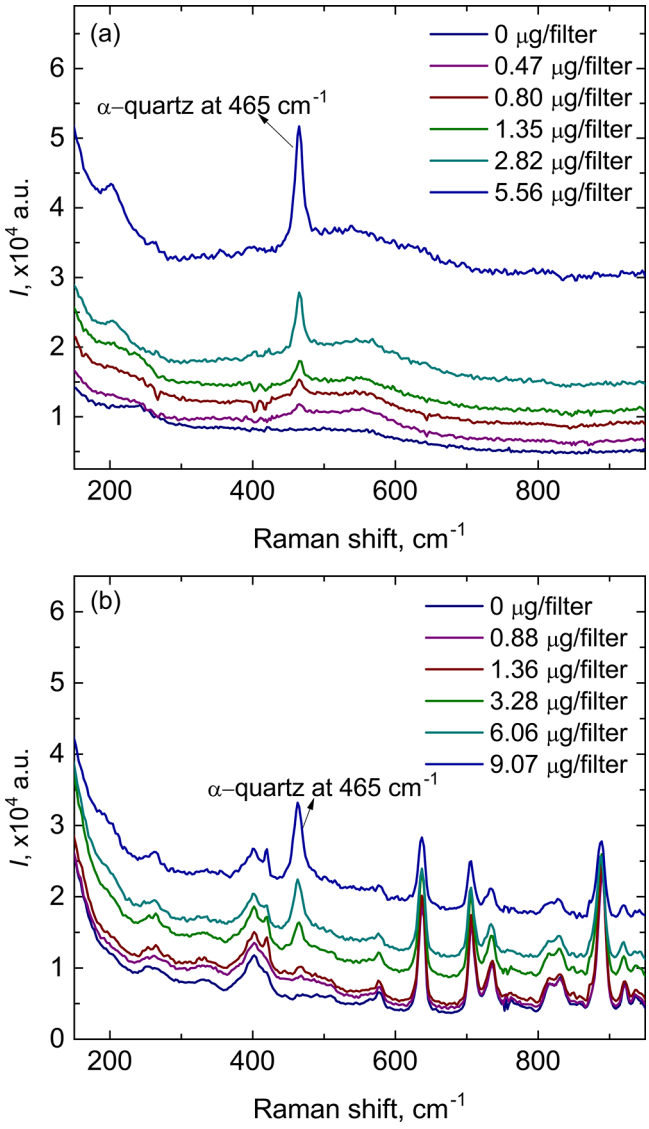

Figure 3. Raman spectra of α-quartz deposited on silver (a) and PC (b) filters at different mass loadings using collection method A (i.e., focused collection using a nozzle). Measurement integration time was 30 s.

that the spatial distribution of the analyte is uniform over the entire spot. The spot size from the three methods and the corresponding variation of mass density within the spot were investigated using scanning electron microscopy (SEM) and spatially resolved Raman spectroscopy. To quantitatively describe the deposition uniformity, Raman spectra were measured at various locations along a preselected axis of the sample spot. Figure 4 shows SEM images (a–c) of sample spots of α-quartz deposited on silver filters and the corresponding variation of peak Raman signal intensity (d–f) of α-quartz as a function of location of the sample probed by the laser using collection methods A–C.

Method A, involving direct aerosol collection via a nozzle, leads to a smeared circular deposit, with an approximate diameter of 0.8 mm (Figure 4a). The smeared collection of particles is likely due to particle bounce, broad distribution in particle Stokes number in the aerosol sample, and flow expansion at the nozzle outlet. Better focusing could be achieved by using alternate focusing techniques involving

DOI: 10.1021/acs.analchem.8b00830
Anal. Chem. 2018, 90, 6229–6239

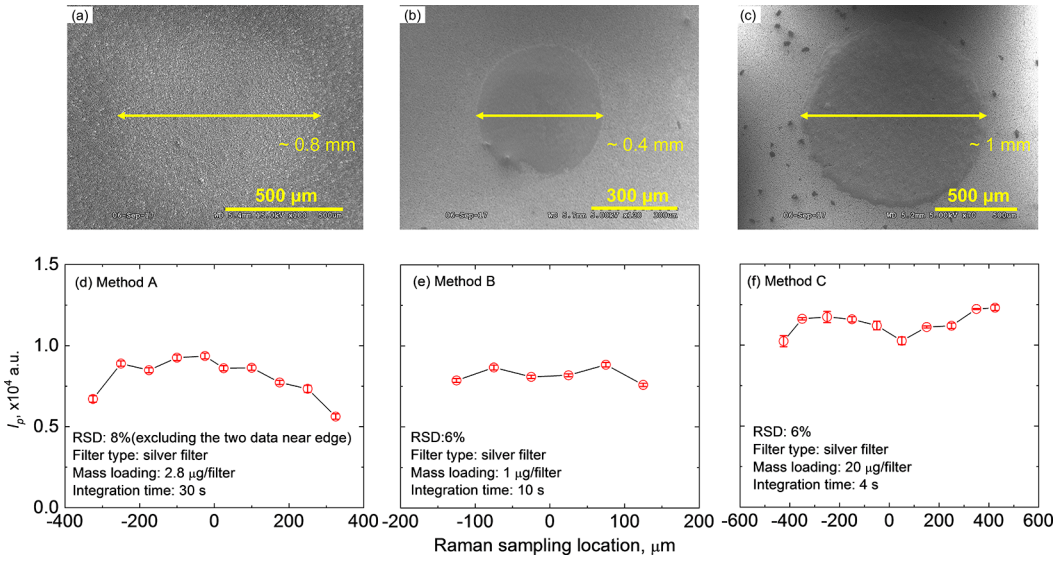

Figure 4. SEM images (top row: a–c) of particulate α-quartz deposited on silver filters and variation of Raman signal intensity (bottom row: d–f) of α-quartz as a function of sampling location using methods A–C (the center of each deposit is located at 0 mm).

multiple nozzles[36] or orifices[37] that allow focusing of wider range of Stokes number. For method A, the Raman signal intensity acquired near the edge of the spot was lower than that near the center of the spot (Figure 4d). The relative standard deviation (RSD) of the mean Raman signal intensity for method A was 8% (excluding the two locations near the edge of the deposit).

Method B involved collection using a Spotsampler device, in which the smaller particles (of the sampled aerosol) were grown into larger droplets (>1 μm) in a supersaturated atmosphere of water vapor. The grown droplets were then focused and collected on an impaction plate using a nozzle. The sample spot diameter using this method was approximately 400 μm (Figure 4b). From Raman analysis, method B appears to provide relatively uniform spatial density of analyte mass (Figure 4e); the RSD of the mean Raman signal intensity for method B was 6%.

The dried spot obtained by method C has a well-defined diameter of 1 mm (Figure 4c), which is same as the diameter of masking orifice plates used during syringe filtration (note: the dark spots around the deposit in Figure 4c are likely contaminant particles from the 3D printed masking orifice plate, which is made of polymer resin). From Raman analysis, method C also provides relatively uniform spatial density of the analyte mass (Figure 4f). The RSD of the mean Raman signal intensity for method C was 6%.

Calibration. From the Raman spectra of α-quartz shown in Figure 3, it was observed that at a given signal integration time, the baseline of the Raman spectra shifted upward with increasing mass loading on the filter, reaching detector saturation beyond a certain high mass loading. At such high mass loading, it is essential to reduce integration time to reduce collection of excess Rayleigh scattered light. On the other hand, increasing integration time is necessary to detect low analyte mass. A range of integration times would be required to measure samples with a range of mass loading. Constructing calibration curves that could be applied to Raman measurements with different integration times is useful for quantitative analysis.

First, the effect of integration time on the signal intensity and the signal-to-noise ratio (SNR) was investigated. Figure 5a shows Raman spectra of 5 μg of α-quartz deposited on a silver filter at different signal integration times. As the integration time increases, the α-quartz signal increases. Figure 5b shows the α-quartz signal intensity and the SNR plotted as a function of integration time. The error bars show the standard deviation of the signal intensity for replicate measurements (n = 5). The SNR was calculated as the average peak height over five repeat measurements, divided by the standard deviation of the peak height.[38] Both the signal intensity and the SNR increase with the integration time. The signal intensity is directly proportional to the integration time, with R^2=0.9984. However, the relationship between the SNR and the integration time is nonlinear because the noise increases with the integration time. The SNR data was fitted with a general expression:

$$\mathrm{SNR} = \frac{I_p}{\sigma} = \frac{I_p}{(\sigma_I^2 + \sigma_B^2 + \sigma_d^2 + \sigma_r^2)^{1/2}} \quad (1)$$

where I_p is signal, σ_I is signal shot noise ($I_p^{1/2}$), σ_B is background shot noise, σ_d detector dark noise, and σ_r is readout noise.[38] σ_r is independent of integration time. σ_B^2 and σ_d^2 are proportional to integration time (t) and are lumped into a single term in the best-fit equation for SNR shown in Figure 5b. The above equation suggests that the noise was dominated by shot noise (σ_I, σ_B, and σ_d) at integration times greater than ~3 s. The shaded areas for the fitting curves in Figure 5b represent the 95% confidence limits about the curves. Higher SNR at longer integration time demonstrated that lower detection limits could be achieved by increasing integration time, which is particularly important for detecting low mass loadings.

Calibration curves for α-quartz were constructed by plotting the signal intensity obtained at fixed integration times as a function of mass loading deposited on filters. Figure 6a shows calibration curves for α-quartz constructed with different integration times (4, 7.5, 15, and 30 s) using sample preparation method C and a 1.5 mm diameter deposition spot. The integration time was chosen depending on the mass loading. For lower mass loadings, a longer integration time was used, while for higher mass loadings, a shorter integration time

DOI: 10.1021/acs.analchem.8b00830
Anal. Chem. 2018, 90, 6229–6239

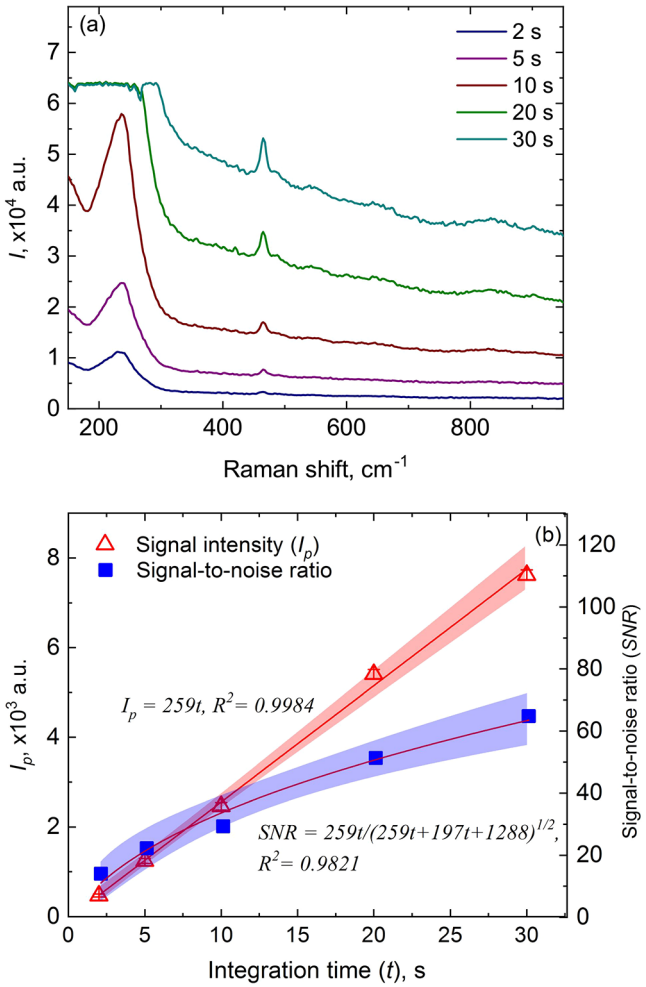

Figure 5. (a) Raman spectra of 5 μg α-quartz over a 1.5 mm diameter spot deposited on a silver filter obtained at different integration times; and (b) variation of the peak signal intensity and the corresponding signal-to-noise ratio as a function of signal integration time using sample preparation method C.

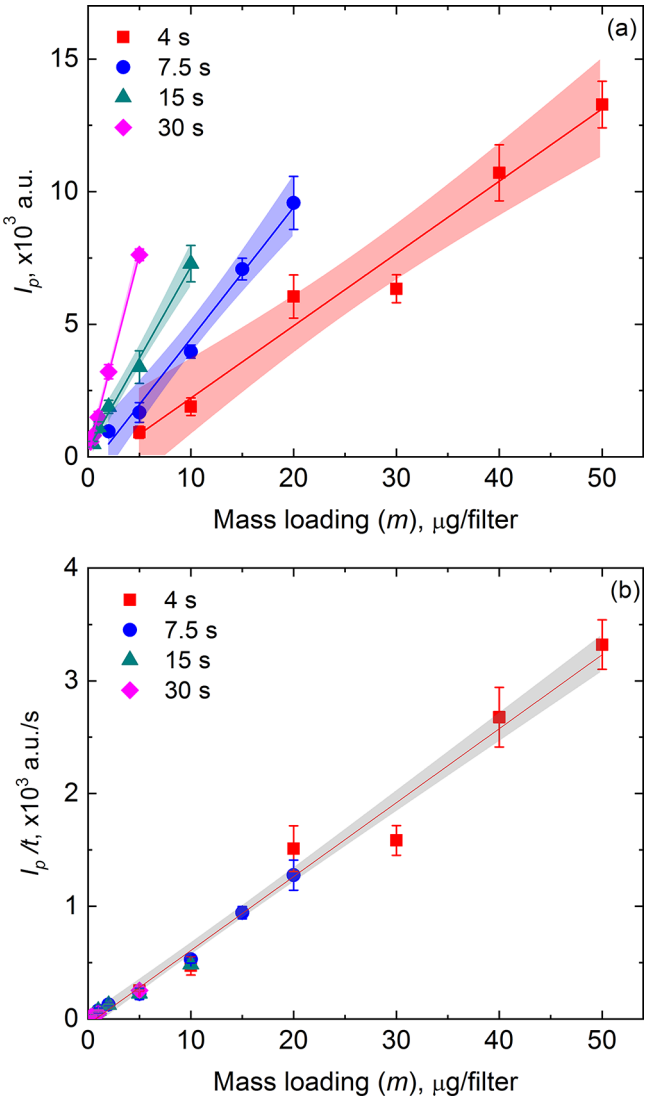

Figure 6. (a) Calibration curves constructed by plotting peak signal intensity as a function of mass loading per filter obtained at different sample integration times (4, 7.5, 15, and 30 s); (b) Calibration curve constructed by plotting peak signal intensity per unit time as a function of mass loading per filter. The sample was deposited over a 1.5 mm diameter spot on a silver filter using sample preparation method C. The lines represent linear fits to the experimental data.

was used. For example, an integration time of 30 s was used for constructing a calibration curve with a mass loading range of 0.25−5 μg, and an integration time of 4 s was used for constructing a calibration curve in the mass loading range 5−50 μg. As shown in Figure 6a, the sensitivity increases with increasing integration time when all other conditions remain the same. The data in Figure 6a can be collapsed into one curve when plotted as signal intensity per unit time versus the mass loading deposited on filters, as shown in Figure 6b. The signal intensity per unit time is directly proportional to the mass loading for a given deposition area, which can be expressed as

$$I_p/t = S'm \quad (2)$$

where I_p is the Raman signal intensity for α-quartz, t is the integration time (s), m is the mass loading (μg), and S' is the slope of the calibration curve in Figure 6b. The calibration curve showing signal intensity per unit time as a function of mass loading is suitable for measuring α-quartz mass loading in a range of 0.25−50 μg by using integration times ranging from 4 to 30 s. Lower or higher mass loadings can be measured by further increasing or decreasing the integration time accordingly.

Figure 7a shows three calibration curves showing signal intensity per unit time as a function of mass loading, constructed for 1, 1.5, and 3 mm diameter deposition spots. All three curves can be expressed using eq 2. As expected, the sensitivity increases with decreasing deposition diameter because the surface mass density (i.e., the mass per unit deposition area) is higher at a smaller sample spot size for a given analyte mass deposited on the filter. The data in Figure 7a can be collapsed into one curve when plotting signal intensity per unit time as a function of surface mass density, and is shown in Figure 7b. The signal intensity per unit time is directly proportional to the mass loading per unit area up to 30 μg/mm^2 (corresponding to deposit thickness of approximately 12 μm), regardless of the sample spot size (as long as it is greater than the laser beam diameter incident on the filter). The maximum sampling depth is limited by the depth of field of the collection optics, the laser focus depth, the absorption and

DOI: 10.1021/acs.analchem.8b00830
Anal. Chem. 2018, 90, 6229−6239

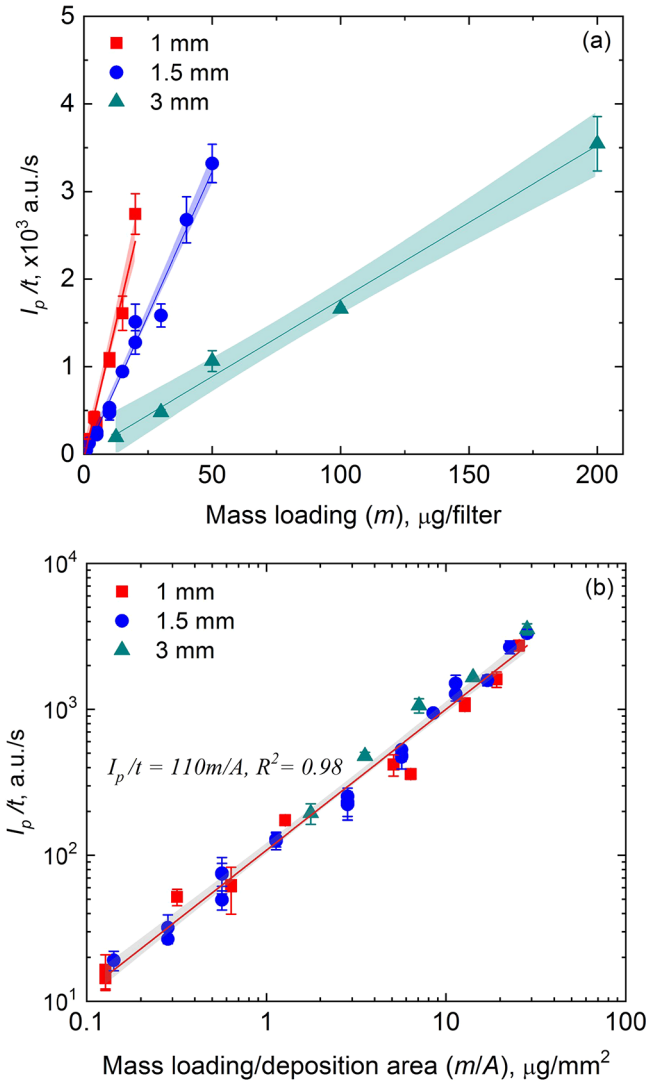

Figure 7. (a) Calibration curves constructed by plotting peak signal intensity per unit time as a function of mass loading deposited on silver filters with different deposition diameters (1, 1.5, and 3 mm) using sample preparation method C; (b) Calibration curve constructed by plotting peak signal intensity per unit time as a function of mass loading per unit area using sample preparation method C. The lines represent linear fits to the experimental data.

scattering properties of the sample.[38] These factors were not investigated in this study. Our results show that a linear calibration curve for measurement of α-quartz can be obtained for samples up to deposit thickness of 12 μm using the Raman instrument used in this study. The calibration curve in Figure 7b can be expressed as

$$I_p/t = S^*\frac{m}{A} \quad \text{or} \quad I_p = \frac{S^*t}{A}m \tag{3}$$

where S^* is the slope of the calibration curve in Figure 7b, and A is the area of sample spot (mm^2). Here, we define S^* as the intrinsic Raman spectroscopic sensitivity. For a given Raman spectroscopic system and a sample substrate, S^* is constant for a given analyte. For our Raman system, S^* for α-quartz was measured to be 110 μg^{-1} s^{-1} mm^2. eq 3 is a universal calibration equation, which can be applied to measurements taken with any combination of signal integration time and sample spot size. From eq 3, the measurement sensitivity (S_m) in terms of mass is then given by

$$S_m = \frac{S^*t}{A} \tag{4}$$

The measurement sensitivity for aerosol analysis using Raman spectroscopy increases with increasing integration time and decreasing deposition area. Using eq 4, measurement sensitivity at various integration times and sample spot sizes can be obtained.

Figure 8 shows calibration curves constructed by plotting signal intensity per unit time as a function of mass loading

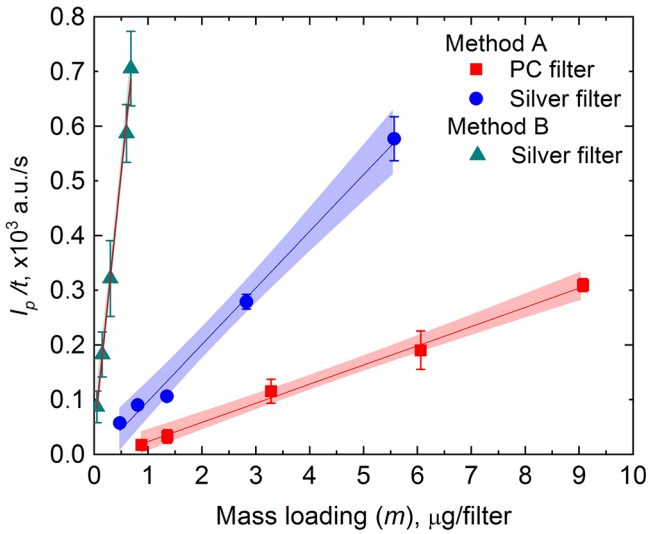

Figure 8. Calibration curves constructed by plotting peak signal intensity per unit time as a function of mass loading deposited on silver and PC filters using sample preparation methods A and B.

deposited on silver and PC filters using sample preparation methods A and B. For silver filters used as a deposition substrate, the slope of the calibration curve using method A is close to that using method C with 1 mm diameter deposition. Although the sample spot size using method A is smaller than 1 mm, its measurement sensitivity is lower than that of the method C using 1 mm sample spot diameter. This can possibly be attributed to the smeared deposition of particles in method A (Figure 3). Comparison of the calibration curves for silver and PC filters shows that the silver filters show three times better measurement sensitivity than PC filters. However, silver filters cost significantly more than PC filters. The PC filter could be a cost-effective option for crystalline silica measurement using direct-on-filter Raman measurement. The measurement sensitivity of method B is significantly superior to that of the other two methods, demonstrating the capability of the condensational droplet growth technique for efficient concentration of airborne particles onto a small spot. The calibration data of method B could also be collapsed into a single universal calibration curve shown in Figure 7b, while that of method A could not be collapsed into a single curve due to lack of a clear, well-defined spot size. The shaded areas for the calibration curves in Figures 5−7 represent 95% confidence bands, which increase noticeably with integration time. Each data point on the calibration curves in Figures 5−7 represents the average of three replicate measurements. The error bar represents the standard deviation around the mean. The relative standard

DOI: 10.1021/acs.analchem.8b00830
Anal. Chem. 2018, 90, 6229−6239

deviation (RSD) calculated by three replicate measurements is in the range of 3−25%, with higher RSD for measurements taken for lower mass loadings around the LOQ; the average RSD is approximately 10%, which is satisfactory for routine workplace aerosol exposure measurement.

Effects of particle size on calibration curve characteristics were not investigated in this study. Stowers and Friedlander[23] showed that the integrated Raman scattered intensity over many particles in the scattering volume (~0.02 mm^3) interacting with the laser beam is proportional to the total particulate mass. Stacey et al.[33] have also recently shown that the characteristics of the calibration curve, constructed by plotting the total signal intensity averaged over 50 sampling points (~100 μm^2) in a 5 mm deposit as a function of analyte mass, does not depend on particle size distribution. These results suggest that the influence of particle size distribution on the total Raman scattered signal integrated over a specific volume (for particles in a flowing stream) or area (for particulate samples deposited on a substrate) is minimal, and that the Raman scattering intensity can be assumed to be proportional to the total analyte mass irradiated by the laser beam. This permits application of calibration curves constructed using a standard reference material to all test aerosols studied in this work.

Sample Recovery. The recovery of α-quartz during sample ashing was investigated. For the sample recovery tests, 10 μL aliquots of suspensions of the SRM 1878a material at different concentrations (2, 5, and 10 $\mu g/\mu L$) were pipetted on 25 mm MCE filters. Three replicates were prepared for each mass loading. The filter samples were pretreated using low-temperature plasma ashing and subsequently analyzed by Raman spectroscopy using method C described earlier. Calibration curves in Figure 7b were used to obtain mass loadings. The recoveries were found to be 95%, 103%, and 97% for 20, 50, and 100 μg mass loadings, respectively. Because recoveries were close to 100%, no recovery correction factor was used to adjust the measurement results.

Detection Limits. The limit of detection (LOD, m_{LOD}) was estimated using 3-σ criteria defined by the International Union of Pure and Applied Chemistry (IUPAC) as[39]

$$m_{LOD} = 3\sigma/S_m \quad (5)$$

where σ is the standard deviation of the blank at the selected spectral region and S_m is the measurement sensitivity in terms of mass loading. Both σ and S_m varied with integration time (Figures 6−8). Blank measurements were taken in the absence of any analyte deposited on the filter, following identical measurement procedures as those used for samples containing α-quartz. The standard deviation of the blank was calculated from spectra obtained from 15 randomly selected locations on three separate blank filters. The LODs for different methods at different integration times are shown in Table 1. With an integration time of 60 s, the LOD in terms of mass is 0.074 μg using method A, 0.008 μg using method B, and 0.055 μg using method C (for 1 mm spot diameter). The LODs obtained by our Raman methods are two to three orders of magnitude lower than currently used standardized methods, such as X-ray diffraction[5] and infrared spectroscopy.[6]

Stacey et al. reported an LOD of 0.02 μg of α-quartz per filter by analyzing 50 sampling points on a 5 mm diameter filter deposit.[33] Assuming the deposition was uniform, we estimated the LOD of their Raman method, in terms of mass per unit sample area, to be about 0.001 $\mu g/mm^2$ (obtained by dividing the LOD per filter by the sample deposition area), whereas our method provides an LOD of 0.46 $\mu g/mm^2$ at an identical signal integration time. The micro-Raman system used by Stacey et al. (In-Via Raman microscope [Renishaw Ltd., Gloucester, U.K.], with near-IR (785 nm) laser excitation, CCD camera, and a 1200 l mm^{-1} grating) is a highly sensitive laboratory instrument, while a field-portable instrument was used in our study. Even with more than 2 orders of magnitude lower sensitivity of our portable Raman method, comparable detection limits (in terms of mass per filter) could be achieved by efficient aerosol microconcentration techniques. This underscores the importance of microconcentration for Raman analysis.

Table 1. Limits of Detection for Spectrometric Determination of α-Quartz Obtained by Three Different Methods at Different Integration Times

	limits of detection, μg				
	focused collection using nozzle (method A)	focused collection using *Spotsampler* (method B)	redeposition through narrow orifice (method C)		
integration time, s	0.8 mm	0.4 mm	3 mm	1.5 mm	1 mm
5	0.49	0.053	3.277	0.819	0.364
15	0.198	0.022	1.324	0.331	0.147
30	0.116	0.013	0.778	0.194	0.086
60	0.074	0.008	0.495	0.124	0.055

Feasibility of near Real-Time Raman Measurement. Collection techniques A and B were designed to probe their usefulness for direct, near real-time analysis of workplace aeosols. A near real-time scheme using these techniques would involve collection, on either a rotating filter disc or moving linear tape, to allow sampling followed by immediate in situ analysis, rendering near real-time measurement capability. Though such an automated sampling and analytical scheme was not investigated in this study, the LODs established for techniques A and B can provide estimates of time resolution and detection limits (in terms of air concentrations) for such a near real-time measurement scheme. Alternatively, the universal calibration curve shown in Figure 7b can be used to determine the sample spot size that would allow near real-time measurement. Table 2 shows the limits of quantification (LOQ; 3.3 × m_{LOD}) for methods A and B at sample collection times of 5 and 10 min. A flow rate of 1.2 L/min and a Raman integration time of 60 s was assumed in the calculations. Typical sampling flow rates for cyclone samplers are about 2 or 4 L/min; higher flow samplers enabling up to about 10 L/min are also available and can be used to further lower the LOQ (below those reported here) for short-term monitoring, if needed. The results demonstrate that the LOQs are low enough to allow near real-time measurement of airborne crystalline silica concentrations in typical workplaces.

Table 2. Estimated LOQs for α-Quartz in Terms of Air Concentration, Obtained by Methods A and B

	LOQ, $\mu g/m^3$	
collection time, min	method A	method B
5	37	4
10	18.5	2

DOI: 10.1021/acs.analchem.8b00830
Anal. Chem. 2018, 90, 6229−6239

Comparison of Aerosol Microconcentration Techniques. Each of the three sample concentration methods developed in this study offers unique advantages and disadvantages. Methods A and B are direct on-filter analysis techniques, wherein the aerosol sample is collected on a filter and analyzed directly by a Raman probe without any sample pretreatment. The direct on-filter analytical approach is also commonly used for crystalline silica measurement using XRD and IR techniques.[12,40] Direct on-filter methods can minimize measurement errors caused by analyte loss in the pretreatment process and can provide instant results for field measurement when portable instruments are used. However, depending on the nature of the aerosol, matrix interferences can increase measurement uncertainty when using methods A and B. We anticipate that the detection limit of method A could be further reduced by using improved focusing techniques involving multiple nozzles[36] or orifices.[37]

Of the three methods studied here, method B offers the most effective microconcentration capability and provides the lowest detection limits for α-quartz. However, this method involves a relatively large apparatus required for growing the sampled particles to form droplets. Method C is a laboratory analysis method, requiring a sample pretreatment and redeposition process. Method C allows measurement of α-quartz in complex samples with potential matrix interferences. This sample pretreatment procedure has also been employed by current standardized methods for RCS measurement, such as NIOSH methods 7500 and 7603.[8,9] The microconcentration of collected aerosol in method C is accomplished using filtration through an orifice. A smaller orifice (<1 mm) can provide better detection limits; however, this is achieved at the expense of a slower rate of filtration of the analyte suspension.

Measurement of Workplace Samples. Techniques A and C were applied to the measurement of two types of workplace aerosol samples: sample #1 was collected during an actual cutting operation (using a power tool) of a stone countertop at a fabrication facility; sample #2 was collected during cutting (using a power saw blade) of fiber cement siding at a construction site. Sample #1 contained ~90% α-quartz and resins, polymers, and pigments;[41] sample #2 contained a small percentage of α-quartz ranging from 10 to 30%, along with other matrix components such as cellulose fibers and cement.[42] The representative Raman spectra for samples #1 and #2 are shown in Figure 9a. No spectral interference was observed for the α-quartz peak at 465 cm^{-1}. The workplace samples, which were in the form of powders, were aerosolized using a fluidized bed aerosol generator (TSI, Inc.) to generate test aerosols with different air concentration levels of α-quartz. A respirable fraction[43] of this test aerosol was collected and subsequently measured using Raman spectroscopy using techniques A and C, as well as NIOSH method 7500.

NIOSH method 7500 involved filter dissolution using tetrahydrofuran, redeposition on a silver filter and subsequent analysis by XRD. Test aerosols with relatively high concentration levels were collected for 2 min at 1.2 L/min for method A and at 2 L/min for method C, and collected for 10 min at 2 L/min for NIOSH method 7500. For measuring the low concentration aerosol, the collection time was 10 min for method A and C, and 2 h for NIOSH method 7500. The concentrations of α-quartz in test aerosols were in the range 30–2000 $\mu g/m^3$. Aerosol samples with α-quartz concentrations less than 30 $\mu g/m^3$ were not tested because their mass loading

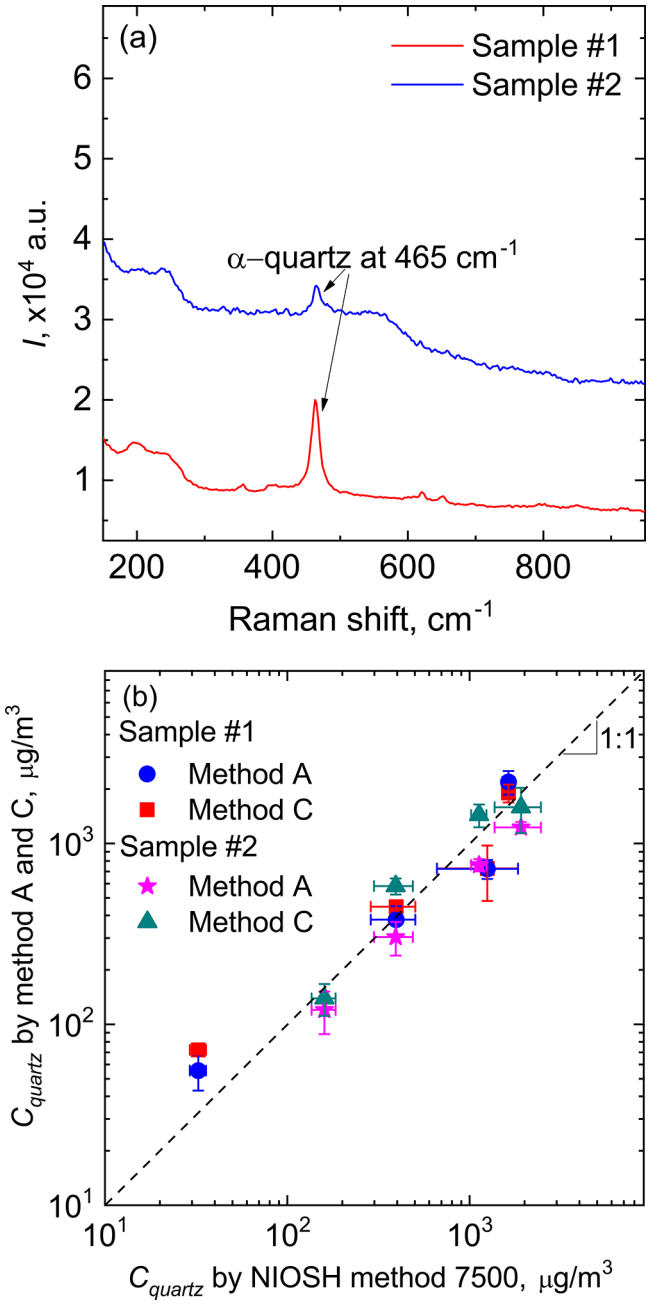

Figure 9. (a) Representative Raman spectra for sample #1 (aerosol generated during stone cutting operation using a power tool) and sample #2 (aerosol generated during cutting of fiber cement sidings); (b) Comparisons of airborne α-quartz concentrations in laboratory-generated aerosol samples #1 and #2, measured by method A, method C, and NIOSH method 7500.

obtained by 2-h collection would be below the LOQ of the reference XRD method.[8]

Figure 9b shows comparisons of airborne α-quartz concentrations in samples #1 and #2, measured by methods A and C, and NIOSH method 7500. The vertical error bars in Figure 9b show the standard deviations of three replicate measurements by methods A and C, and the horizontal error bars show the standard deviations of three replicate measurements by NIOSH method 7500. In general, the results from methods A and C agreed well with those from NIOSH method 7500, demonstrating accuracy of our Raman methodology. The

DOI: 10.1021/acs.analchem.8b00830
Anal. Chem. 2018, 90, 6229–6239

RSDs for methods A and C were in a range of 5−30%, comparable to the intralaboratory measurement precision (8−28%) of NIOSH method 7500.[8]

The normalized root-mean-square error (NRMSE = RMSE/($y_{max} - y_{min}$), where RMSE is root mean squared error) was used to estimate the differences between our methods and NIOSH method 7500. For sample #1, the NRMSE was 24% for method A and 18% for method C. For sample #2 (fiber cement), the NRMSE was 23% for method A and 14% for method C. The direct-on-filter measurement method (method A) gave poorer accuracy than method C, which involves sample pretreatment. Two-factor analysis of variance (ANOVA) with replication was used to test the difference among methods. Analysis of α-quartz in sample #1 showed no statistically significant difference between method A, method C and NIOSH method 7500 ($F(2, 16) = 0.16$, $p > 0.05$). An ANOVA of results for sample #2 showed no statistically significant difference between method C and method 7500 ($F(1, 16) = 0.001$, $p > 0.05$), but showed a statistically significant difference between method A and the NIOSH method ($F(1, 16) = 13.9$, $p < 0.05$). For sample #2, method A provided significantly lower values than method C and the NIOSH method, perhaps due to matrix interferences and lower quartz content. These biases can likely be reduced by constructing calibration curves using the actual material (to account for matrix effects), instead of the pure crystalline silica (as was done in this study).

Matrix and Mineral Interferences. Interference from various constituents of the collected particulate matter could potentially affect the Raman measurement. These interfering species could be components of outdoor atmospheric aerosols, such as secondary organic aerosols, nitrates, sulfates, or PAHs, or from indoor/workplace air such as soot or diesel particulate matter. Table S1 in the SI lists the peak Raman frequency shifts for the major components of the atmospheric aerosol. The Raman-active modes associated with key organic species (e.g., C−C, C−H, C═O, OH) and inorganic species (e.g., NO_3^-, NH_4^+, CO_3^{2-}) have characteristic peaks at wavenumbers beyond 1000 cm^{-1},[13,14,44−47] and are not likely to interfere with the α-quartz peak. Sulfates, however, show a peak at ∼450 cm^{-1},[45] which partially overlaps with the α-quartz peak at 465 cm^{-1}. Depending on the degree of overlap, these peaks could be deconvoluted using peak fitting to separate Raman signals of α-quartz and sulfates. We did not investigate sulfate interference in this study. Since the concentration of atmospheric aerosol is usually much lower than the workplace aerosol concentration, the potential spectral interferences are likely negligible for most workplaces. Method C in this study, which pretreats the sample using low-temperature ashing in oxygen plasma, can significantly reduce matrix interference for many aerosols.

Interference from other inorganic mineral constituents in the particulate phase could also affect the measurement of α-quartz. Quartz is a common component of workplace aerosols, which are mechanically generated from soil, rocks, sand, cement, glass, porcelain, and brick. Cristobalite, a polymorph of crystalline silica, is less common; tridymite, another polymorph, is even rarer to find in workplace aerosols.[6] Kaolinite is also an interfering mineral found in some bituminous coal aerosols.[6] Cristobalite, tridymite, and kaolinite all have overlapping Raman peaks that could potentially interfere with α-quartz measurement.[48,49] Table S2 in the SI lists peak Raman frequency shifts for potential interfering minerals of geological origin. Infrared methods for α-quartz correct for positive interference from these minerals by determining content of interfering mineral by using a noninterfering absorption peak.[6] Similar correction procedures could be implemented for α-quartz measurement using the Raman method.

CONCLUSIONS

Aerosol microconcentration techniques have been successfully coupled with micro-Raman spectroscopy to achieve measurement of trace crystalline silica in air. The techniques used in this study allow deposition of aerosol samples as a spot with a diameter ranging from 400 to 3000 μm, thereby significantly improving the detection limits. A universal calibration curve for α-quartz was developed by plotting the signal intensity per unit integration time as a function of mass per unit sample spot area, which allowed choosing any combination of sample spot size and Raman signal integration time for Raman analysis. This universal calibration curve can also be used to determine the sample spot size that would allow near real-time measurement. Our methods provided detection limits in the range of 8−55 ng α-quartz with a sample spot diameter of 400−1000 μm and a sample integration time of 60 s. The detection limits are two to three orders of magnitude lower than those attainable from current standardized XRD and IR methods. The direct-on-filter method used in this study can provide an LOQ of 18.5 $\mu g/m^3$ using a focusing nozzle (i.e., method A) and 2 $\mu g/m^3$ using the Spotsampler (i.e., method B) at a time resolution of 10 min, thereby allowing near real-time measurement of airborne crystalline silica concentration.

Both direct-on-filter and indirect (i.e., after sample pretreatment) methods were successfully applied to measurement of workplace aerosol samples containing α-quartz. Comparison of our Raman measurements after sample pretreatment (method C) with those from the NIOSH method 7500 showed no statistically significant difference, while the measurements from our direct-on-filter method (method A) and NIOSH method 7500 showed statistically significant differences for a sample with a lower α-quartz content and a complex matrix. Thus, for some sample matrices, a direct-on-filter method may require a calibration procedure that accounts for potential matrix effects on the analyte signal. The study demonstrates that efficient microconcentration of aerosol particles can achieve very low detection limits when using field-portable Raman spectrometers.

ASSOCIATED CONTENT

Supporting Information

The Supporting Information is available free of charge on the ACS Publications website at DOI: 10.1021/acs.analchem.8b00830.

Experimental scheme used for collecting aerosol test samples; Laser-induced sample heating; Peak Raman frequency shifts for potentially interfering species (PDF).

AUTHOR INFORMATION

Corresponding Author

*Phone: (513) 841-4300. Fax: (513) 841-4545. E-mail: pskulkarni@cdc.gov.

ORCID

Pramod Kulkarni: 0000-0001-7692-4662

DOI: 10.1021/acs.analchem.8b00830
Anal. Chem. 2018, 90, 6229−6239

Notes

The findings and conclusions in this paper are those of the authors and do not necessarily represent the views of NIOSH. Mention of company names and products does not constitute endorsement by NIOSH.

The authors declare no competing financial interest.

■ ACKNOWLEDGMENTS

This research work was supported by a NIOSH intramural NORA grant. The authors thank Dr. John Snawder, Dr. Rosa Key-Schwartz, and Dr. Robert Streicher for valuable feedback on this manuscript. We also thank Dr. Chaolong Qi for providing workplace samples and Dr. Chen Wang for conducting electron microscopy of filter samples.

■ REFERENCES

(1) Esswein, E. J.; Breitenstein, M.; Snawder, J.; Kiefer, M.; Sieber, W. K. *J. Occup. Environ. Hyg.* **2013**, *10*, 347−356.
(2) NIOSH, *NIOSH Hazard Review − Health Effects of Occupational Exposure to Respirable Crystalline Silica*; DHHS: Cincinnati, 2002.
(3) OSHA, *Occupational Exposure to Respirable Crystalline Silica*; Final Rule; Fed. Regist., 2016.
(4) Yassin, A.; Yebesi, F.; Tingle, R. *Environ. Health Perspect.* **2004**, *113*, 255−260.
(5) ISO. Workplace Air − Analysis of Respirable Crystalline Silica by X-ray Diffraction (2 parts). *ISO 16285*; ISO, Geneva, Switzerland, 2015.
(6) ASTM. *ASTM D7948 Standard Test Method for Measurement of Respirable Crystalline Silica in Workplace Air by Infrared Spectrometry*; ASTM International: W. Conshohocken, PA, 2014.
(7) NIOSH. 7602 - SILICA, Respirable Crystalline, by IR (KBr pellet). *NIOSH Manual of Analytical Methods*, 5th ed.; DHHS: Cincinnati, 2017.
(8) NIOSH. 7500 - Silica, Crystalline, by XRD (filter redeposition). *NIOSH Manual of Analytical Methods*, 4th ed.; DHHS: Cincinnati, 2003.
(9) NIOSH. 7603 - QUARTZ in Respirable Coal Mine Dust, by IR (Redeposition). *NIOSH Manual of Analytical Methods*, 5th ed.; DHHS: Cincinnati, 2017.
(10) Madsen, F. A.; Rose, M. C.; Cee, R. *Appl. Occup. Environ. Hyg.* **1995**, *10*, 991−1002.
(11) Miles, W. J. *Am. Ind. Hyg. Assoc. J.* **1999**, *60*, 396−402.
(12) HSE. MDHS101/2 - Crystalline silica in respirable airborne dusts: Direct-on-filter analyses by infrared spectroscopy or X-ray. *Methods for the Determination of Hazardous Substances (MDHS) guidance*; HSE: U.K..
(13) Craig, R. L.; Bondy, A. L.; Ault, A. P. *Anal. Chem.* **2015**, *87*, 7510−7514.
(14) Fu, Y.; Kuppe, C.; Valev, V. K.; Fu, H.; Zhang, L.; Chen, J. *Environ. Sci. Technol.* **2017**, *51*, 6260−6267.
(15) Rosasco, G.; Etz, E.; Cassatt, W. *Appl. Spectrosc.* **1975**, *29*, 396−404.
(16) Kalume, A.; Beresnev, L. A.; Santarpia, J.; Pan, Y.-L. *Appl. Opt.* **2017**, *56*, 6577−6582.
(17) Sivaprakasam, V.; Hart, M. B.; Eversole, J. D. *J. Phys. Chem. C* **2017**, *121*, 22326−22334.
(18) Doughty, D. C.; Hill, S. C. *J. Quant. Spectrosc. Radiat. Transfer* **2017**, *188*, 103−117.
(19) Ivleva, N.; McKeon, U.; Niessner, R.; Pöschl, U. *Aerosol Sci. Technol.* **2007**, *41*, 655−671.
(20) Rosen, H.; Novakov, T. *Atmos. Environ.* **1978**, *12*, 923−927.
(21) Fung, K.; Imre, D.; Tang, I. *J. Aerosol Sci.* **1994**, *25*, 479−485.
(22) Sinanis, S.; Aleksandrova, M.; Schaber, K. *Aerosol Sci. Technol.* **2011**, *45*, 751−757.
(23) Stowers, M.; Friedlander, S. *Aerosol Sci. Technol.* **2002**, *36*, 48−61.
(24) Diwakar, P.; Kulkarni, P.; Birch, M. E. *Aerosol Sci. Technol.* **2012**, *46*, 316−332.
(25) Diwakar, P. K.; Kulkarni, P. *J. Anal. At. Spectrom.* **2012**, *27*, 1101−1109.
(26) Zheng, L.; Kulkarni, P.; Birch, M. E.; Deye, G.; Dionysiou, D. D. *Aerosol Sci. Technol.* **2016**, *50*, 1155−1166.
(27) Zheng, L.; Kulkarni, P.; Zavvos, K.; Liang, H.; Birch, M. E.; Dionysiou, D. D. *J. Aerosol Sci.* **2017**, *104*, 66−78.
(28) Zheng, L.; Kulkarni, P.; Dionysiou, D. D. *J. Anal. At. Spectrom.* **2018**, *33*, 404−412.
(29) Zheng, L.; Kulkarni, P.; Diwakar, P. *Spectrochim. Acta, Part B* **2018**, *144*, 55−62.
(30) Zheng, L.; Kulkarni, P. *Anal. Chem.* **2017**, *89*, 6551−6558.
(31) Wei, S.; Kulkarni, P.; Ashley, K.; Zheng, L. *Sci. Rep.* **2017**, *7*, 13860.
(32) Kingma, K. J.; Hemley, R. J. *Am. Mineral.* **1994**, *79*, 269−273.
(33) Stacey, P.; Mader, K. T.; Sammon, C. *J. Raman Spectrosc.* **2017**, *48*, 720−725.
(34) Hering, S. V.; Spielman, S. R.; Lewis, G. S. *Aerosol Sci. Technol.* **2014**, *48*, 401−408.
(35) Santoro, G.; Yu, S.; Schwartzkopf, M.; Zhang, P.; Koyiloth Vayalil, S.; Risch, J. F.; Rübhausen, M. A.; Hernández, M.; Domingo, C.; Roth, S. V. *Appl. Phys. Lett.* **2014**, *104*, 243107.
(36) Vidal-de-Miguel, G.; de la Mora, J. F. *Aerosol Sci. Technol.* **2012**, *46*, 287−296.
(37) Liu, P.; Ziemann, P. J.; Kittelson, D. B.; McMurry, P. H. *Aerosol Sci. Technol.* **1995**, *22*, 293−313.
(38) McCreery, R. L. *Raman Spectroscopy for Chemical Analysis*; John Wiley & Sons, 2005; Vol. *225*.
(39) Boumans, P. *Anal. Chem.* **1994**, *66*, 459A−467A.
(40) Miller, A. L.; Weakley, A. T.; Griffiths, P. R.; Cauda, E. G.; Bayman, S. *Appl. Spectrosc.* **2017**, *71*, 1014−1024.
(41) Johnson, D. L.; Phillips, M. L.; Qi, C.; Van, A. T.; Hawley, D. A. *Ann. Work Expo. Health* **2017**, *61*, 711−723.
(42) Qi, C.; Echt, A.; Gressel, M. *Ann. Occup. Hyg.* **2016**, *60*, 220−230.
(43) John, W. S. Sampling Respirable and Fine Aerosol. In *Particle Size-Selective Sampling for Particulate Air Contaminants*; Vincent, J. H., Ed.; American Conference of Governmental Industrial Hygienists (ACGIH): Cincinnati, 1999.
(44) Ault, A. P.; Zhao, D.; Ebben, C. J.; Tauber, M. J.; Geiger, F. M.; Prather, K. A.; Grassian, V. H. *Phys. Chem. Chem. Phys.* **2013**, *15*, 6206−6214.
(45) Batonneau, Y.; Sobanska, S.; Laureyns, J.; Bremard, C. *Environ. Sci. Technol.* **2006**, *40*, 1300−1306.
(46) Baustian, K. J.; Cziczo, D. J.; Wise, M. E.; Pratt, K. A.; Kulkarni, G.; Hallar, A.; Tolbert, M. A. *J. Geophys. Res. Atmos.* **2012**, *117*, na.
(47) Deng, C.; Brooks, S. D.; Vidaurre, G.; Thornton, D. C. *Aerosol Sci. Technol.* **2014**, *48*, 193−206.
(48) Lafuente, B.; Downs, R. T.; Yang, H.; Stone, N. The power of databases: the RRUFF project. In *Highlights in Mineralogical Crystallography*; Armbruster, T., Danisi, R. M., Eds.; W. De Gruyter: Berlin, Germany, 2015; pp 1−30.
(49) Michaelian, K. *Can. J. Chem.* **1986**, *64*, 285−294.

DOI: 10.1021/acs.analchem.8b00830
Anal. Chem. 2018, 90, 6229−6239